View metadata, citation and similar papers at core.ac.uk
brought to you by CORE
provided by PUblication MAnagement

Structural and Analytical Characterization by Scanning Transmission Electron Microscopy of Silicon-based Nanostructures

A.Armigliato, R.Balboni and A.Parisini

CNR-Istituto IMM, Via P.Gobetti, 101, 40129 Bologna (Italy)

A few recent applications of scanning transmission electron microscopy (STEM) methods to problems of interest for nanoelectronics are reported. They include nanometer-scaled dopant profiles by Z-contrast and strain mapping by convergent beam diffraction.

Introduction

In the present and future CMOS technology, due to the ever shrinking geometries of the electronic devices, the availability of techniques capable of performing a quantitative analysis of the relevant parameters (structural, chemical, mechanical) at a nanoscale is of a paramount importance. The influence of these features on the electrical performances of the nanodevices is a key issue for the nanoelectronics industry (see, e.g. (1))

In this paper it will be reported on the nanoanalysis of two very important physical quantities which need to be controlled in the fabrication processes of nanodevices: the dopant profile in the ultra-shallow Si junctions (USJ) and the lattice strain that generates in the Si electrically active regions of isolation structures. Both these quantities are characterized by methodologies of the scanning transmission electron microscopy (STEM) technique; namely, the dopant profiles are investigated by the so-called Z-contrast annular dark field, (ADF-STEM) method, whereas the mechanical strain will be mapped by the convergent beam electron diffraction (CBED) method. A spatial resolution lower than one nanometer and of a few nanometers can be achieved in the two cases, respectively.

For each of the two methodologies, the paper will first discuss their basic principles. Then, an example of recent applications to the determination of the profile of As, implanted at a low-energy into silicon (Z-contrast), as well as of the two dimensional strain mapping in a shallow-trench isolation (STI) structure (CBED) will be reported.

Dopant Profiles in Silicon by Z-Contrast in HAADF/STEM

Principles of the Method

The Z-contrast ADF-STEM, procedure, applied to the observation of heavily doped implanted Si, was pioneered by S. J. Pennycook and co-workers (2). More recently, this method has been reconsidered by Merli et al. (3,4) and applied to the investigation of ultrashallow junctions in Si using low-energy electrons in a scanning electron microscope, SEM. In those works, the authors arrive at a unified definition of the output signal that in both backscattering electrons BSE and low-energy STEM imaging has a resolution given by the probe size; whereas the signal contrast is found to depend on the interaction volume, in BSE imaging, and on the beam broadening, in STEM. The sensitivity of the method for As and Sb-implanted species was of the order of 1 at. %, while the resolution as defined by the probe size was of the order of 1 nm operating with a SEM equipped

with a Schottky emitter at an energy of 20 kV (4). The results reported here (5,6) represent an extension of this approach to the high-energy STEM case, thus coming back to the original Z-contrast application (2), here redefined and optimized to satisfy some of the new needs of the ultrashallow implants characterization. Among these, the dopant localization at a subnanometer scale, at present only possible with high-energy Z-contrast techniques, as well as the determination of the impurity distribution close to the sample surface. As in previous approaches, we are not attempting to resolve dopant atoms but only to detect the increased electron scattering due to the local dopant concentration over the Si matrix albeit keeping this average localization at the subnanometer scale. Key parameters to achieve this selection of a pure Z-contrast signal, i.e., a signal as much as possible independent of the diffraction contrast contributions of the Si matrix, were found to be the electron probe convergence angle (8 mrad), the inner detector angle (62 mrad), and a slight tilt of the sample away from the <011> cross-section zone axis around the <100> surface normal (5,6). Incident probe size dimensions were kept in between 0.2 and 0.3 nm, as demonstrated by lattice images regularly obtained on crystalline regions when tilting the sample back to the on-axis condition. In the following, contrast profiles related to the atomic number difference between dopant and Si matrix atoms have been calculated from line profiles of the ADF-STEM micrographs averaged over regions about 25 nm wide. The contrast is defined in agreement with Elliot et al. (7) as

$$C(t) = \frac{[I(t) - I_{sub}]}{(I_{sub} - I_{ref})} \qquad [1]$$

where $I(t)$ is the averaged intensity at depth t, I_{sub} is the constant Si substrate intensity and I_{ref} is the reference intensity obtained from a beam-blanked image.

Applications to the case of USJ in As implanted Si.

In the case of 5 keV, 2×10^{15} As^{+}/cm^{2} implantations in Si, the occurrence of an As diffusion towards the surface and a consequent dopant pileup in the surface region has been suggested by secondary ion mass spectroscopy, SIMS, measurements after annealings at 800 °C. However, it is known that SIMS measurements could be affected by some artifacts in proximity of the surface or of the interface with the surface oxide.
To verify the presence of a surface dopant accumulation, ADF-STEM cross-sectional observations have been carried out as preliminarly reported in (5). In Fig. 1a and b, it is shown the typical aspect of the ADF-STEM micrographs taken in on-axis and off-axis sample orientations, respectively. The comparison between these micrographs, taken on the same region of an as-implanted sample, also shows how effectively the diffraction and channeling contrast can be removed by the ADF-STEM micrographs with a slight tilt of the sample. In fact, in the case of the tilted sample, Fig. 1b, a broad intensity maximum is uniquely observed close to the sample surface and even the interface between the amorphized surface region and the Si crystal, Fig. 1a, is no longer visible. In Fig. 2a and b, ADF-STEM micrographs obtained on the implanted samples before and after an annealing at 800 °C for 3 min, respectively, are reported. Three regions can be distinguished based on the visible intensity variations. Starting from the sample surface at the top of the micrographs, a 2 nm wide region corresponding to the Si oxide layer is observed, followed by a brighter doped region whose intensity gradually vanishes, at a depth of about 15 nm, into the darker Si matrix region.

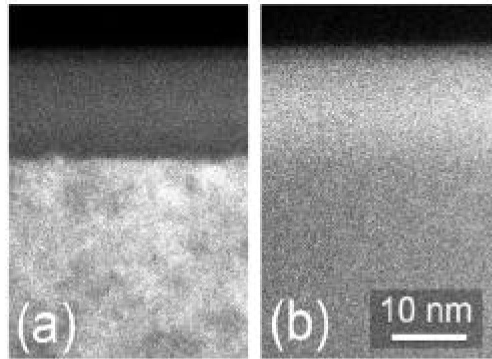

Fig. 1. Z-contrast ADF-STEM micrographs obtained on the same region of a 5 keV $2x10^{15}$ As^{+}/cm^{2} implanted Si sample in on-axis (a) and off-axis (b) sample orientations.

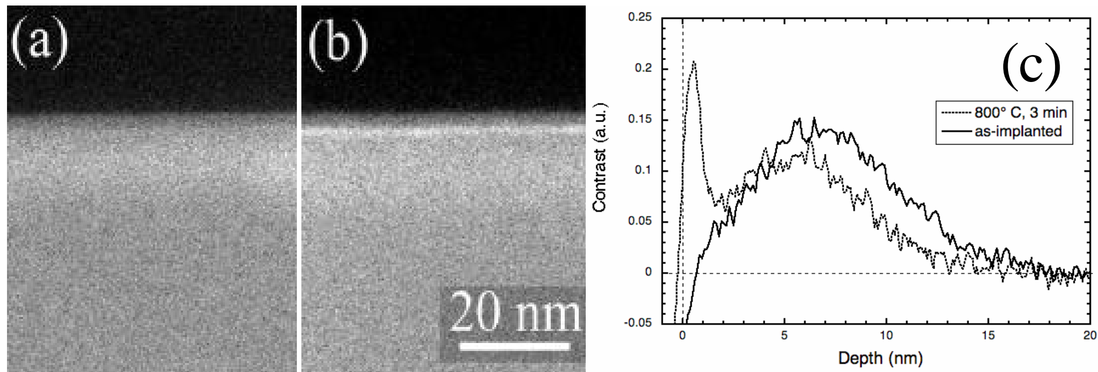

Fig. 2. ADF-STEM micrographs (a, b) and corresponding contrast profiles (c) obtained on 5 keV $2x10^{15}$ As^{+}/cm^{2} implanted Si samples before (a) and after (b) annealing at 800 °C for 3 min.

The contrast profiles reported in Fig. 2c evidence that after the annealing at 800 ° C for 3 min, a pronounced contrast peak close to the sample surface is present. These profiles have been obtained from regions of equal thickness, a relative sample thickness of about 0.7 t/λ (λ is the inelastic electron mean free path, that for pure Si and in our experimental situation corresponds to about 100 nm) being measured in both the cases by parallel electron energy loss spectroscopy, PEELS. Although a detailed investigation of the dependence of these results on the TEM sample thickness has not yet been achieved, we have observed that the effects of the beam broadening on the visibility of the dopant profile become evident for relative specimen thickness $t/\lambda \geq 1.5$. Possible artifacts of the TEM sample preparation have also been excluded by PEELS analyses showing that the surface peak, systematically observed in these experimental conditions, did not correspond to a thicker sample region. The surface contrast peak is thus interpreted as an actual dopant accumulation, confirming the presence of an uphill As diffusion phenomenon. The agreement of both the profiles with the corresponding SIMS profiles is remarkable (5,6) and seems to indicate that, in this case, the sensitivity of the technique is of the order of, or slightly better than, 1 at. %. Finally, it is worth noting that in Fig. 1c, the areas underneath the as-implanted and annealed sample profiles differ by no more than 10%, indicating a constant As dose, at least within the experimental errors. This means that even in the case of ultrashallow junctions, a standardless and quantitative

analysis of impurity concentration should be possible, as originally suggested for shallow implants (2).

Strain Mapping by Convergent Beam Electron Diffraction

Principles of the Method

The convergent beam electron diffraction (CBED) technique of the transmission electron microscopy is presently the only method capable of yielding quantitative strain information with a resolution at the nanometer scale; it is a point-to-point technique, which allows the strain tensor to be obtained at each nanoregion of the sample probed by the electron beam from the analysis of the corresponding diffraction pattern. Basically, the CBED method is based on the strain induced shift of High Order Laue Zones (HOLZ) deficiency lines (8), which occur in the central disk of a convergent-beam pattern, taken in a zone axis where the HOLZ lines are free from dynamical interactions . Due to their high-angle scattering origin, the position of these lines is very sensitive, among other parameters, to small variations in acceleration voltage and lattice parameters (strain). An example of a strain induced HOLZ line shift is given in Fig. 3, which refers to the case of a TEM cross section of a silicon wafer covered with a Si-10 at % Ge film. The HOLZ line pattern taken in the undeformed silicon substrate (left) is clearly different from that taken in the region of the Si-Ge alloy (right). The coherent growth of the film on the substrate results in a tetragonal distortion $\varepsilon_T=6x10^{-3}$. Strains of the order of $2x10^{-4}$ can give rise to a detectable HOLZ lines shift.

In order to quantify the strain, it is first necessary to assess the effective acceleration voltage by matching the pattern taken on the unstrained part of the sample with a kinematically simulated one (9). Then the unknown lattice parameters are determined by fitting the experimental pattern taken on the strained layer with a simulated one, assuming the lattice constants as fitting parameters.

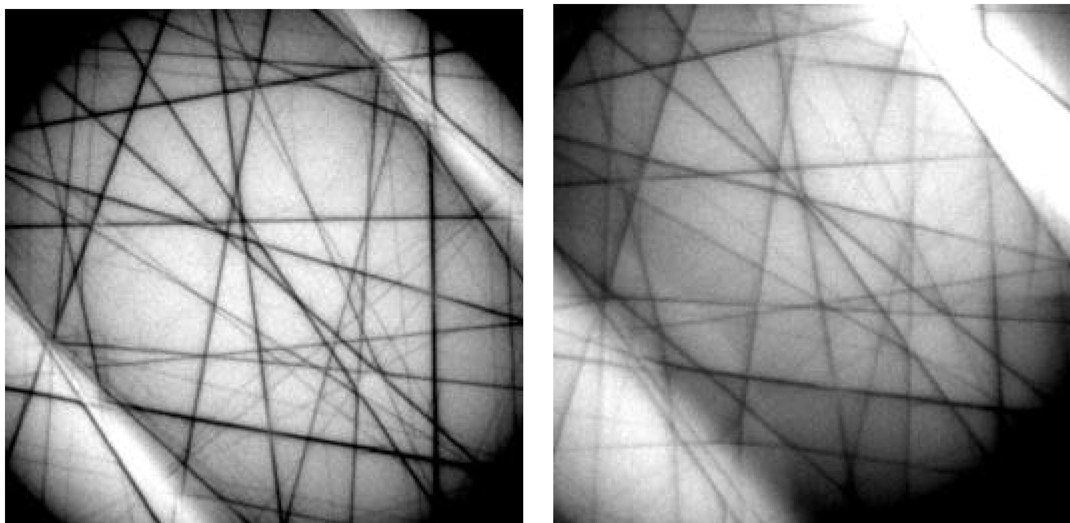

Figure 3. Strain analysis in silicon. Comparison of CBED patterns taken in undeformed silicon (left) and in a highly deformed area of a sample (right). The method is based on the measurement of the shift in the position of the diffraction lines.

This involves first the determination of the position of the HOLZ lines in the experimental patterns, then the extraction of strain tensor from each pattern by comparing it with simulations. The first task is presently accomplished using a dedicated routine (ASAC) in the software iTEM® (by Olympus-SIS (10), which has been developed in the framework of a European project (11), on the basis of the HOLZFIT programme set up in our Institute. The software detects the HOLZ lines by using a formalism similar to the Hough transforms, i.e. all the lines detected in the pattern are represented in a transformed space by their distance from the reference origin and the angle they make with a reference axis. Each pattern is then unambiguously parameterised by computing a set of relevant distances between a number of intersections of the detected HOLZ lines (Fig. 4).

The extraction of the strain tensor is made by comparison of the experimental distance set with the corresponding one obtained by a quasi-kinematical simulation of CBED patterns; the procedure is fully automated and the strained structure which best matches the experimental pattern is extracted using a χ^2 minimisation criterion (12). The effective voltage is calculated by collecting a CBED pattern in the undeformed substrate and simulating it using the voltage as the fitting parameter; then the same voltage is used for the strain tensor calculations. By doing this, all the six lattice parameters are then extracted from a single CBED pattern, as the output of the minimisation routine. The strain tensor component are finally calculated using Equations [2]:

$$\boldsymbol{e}_{XX} = \frac{a_S^X - a_0}{a_0} \qquad \boldsymbol{e}_{XY} = \frac{1}{2}\left(\frac{\boldsymbol{p}}{2} - \boldsymbol{g}_S\right)$$
$$\boldsymbol{e}_{YY} = \frac{a_S^Y - a_0}{a_0} \qquad \boldsymbol{e}_{XZ} = \frac{1}{2}\left(\frac{\boldsymbol{p}}{2} - \boldsymbol{b}_S\right) \qquad [2]$$
$$\boldsymbol{e}_{ZZ} = \frac{a_S^Z - a_0}{a_0} \qquad \boldsymbol{e}_{YZ} = \frac{1}{2}\left(\frac{\boldsymbol{p}}{2} - \boldsymbol{a}_S\right)$$

where X,Y,Z are the crystallographic axes, *S* means strained and *0* undeformed silicon. From these components, the tensor trace Tr(ε) can be simply obtained, as $Tr(\varepsilon)=\varepsilon_{XX}+\varepsilon_{YY}+\varepsilon_{ZZ}$.

In the practical work, the number of unknown parameters must be reduced from 6 (*a*, *b*, *c*, ***a***, ***b***, ***g***) to 3, to obtain a unique solution. As the cross-section orientation is along the [1 1 0] direction, the relations *a*=*b* and Δ***a*** = -Δ***b*** hold. In addition, for the specimen thickness (200-300 nm) used in our CBED experiments, the so called 'planar strain' approximation (i.e. a negligible relaxation in the direction perpendicular to the cross section plane) can be assumed, so Δ*a*/*a*=Δ***g***/2. A detailed explanation of these assumptions has been reported elsewhere (13).

The spatial resolution of the CBED technique is in principle given by the spot size (about 1 nm). This holds along the [0 0 1] direction of the cross-sectioned TEM sample, whereas, due to the sample tilting used in the CBED experiments, the spatial resolution in the [1 -1 0] direction of the TEM cross section perpendicular to the [0 0 1] tilt axis is worsened by the projection effect, which increases with the specimen thickness. For instance, in the case of Fig. 3, as the <230> zone axis is 11.3° off the <110> normal to the plane of the cross section, the spatial resolution in the [1 -1 0] direction is about 10%

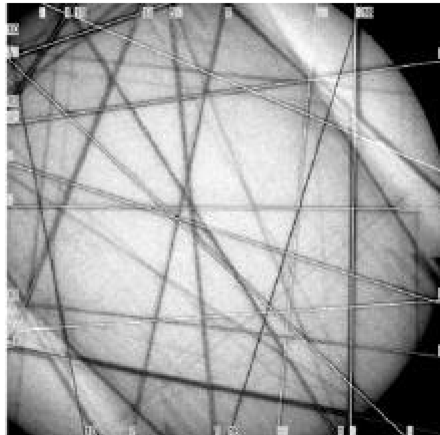

Figure 4. Undeformed silicon CBED pattern (<230>, 200 kV as in Fig. 2); the HOLZ lines skeleton, detected by the ASAC/iTEM® software, is shown superimposed to the experimental lines.

of the local sample thickness, i.e. 20 nm in a 200 nm-thick region of the device. For this reason, it is more convenient to reduce the angle of tilt, and the <340> zone axis (ca. 8° of tilt) has been recently introduced, thus improving the spatial resolution along the [1 -1 0] direction by about 35% with respect to the <230> axis.

Application of STEM/CBED to Strain Maps

The above described method has been so far applied to mapping strain in shallow trench isolation technology of the recent CMOS technology nodes (150-90 nm). The example given here refers to an STI with an active region about 150 nm wide (Fig. 5) and has been chosen to show more clearly the array of analyzed points and of the corresponding values of the trace.

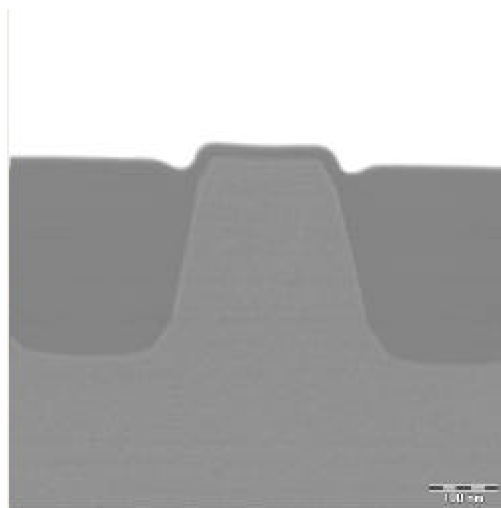

Figure 5. HAADF/STEM image in <110> Si zone axis of an STI structure.

A number of CBED patterns has been taken in points selected by digitally rastering the probe in the 2D region of interest of the cross section; in addition, a CBED pattern in an undeformed area of the substrate is acquired to determine the effective acceleration voltage (9). A database is obtained, consisting of a TEM image with superimposed the matrix of the points selected for CBED pattern acquisition, plus the CBED patterns obtained at each point. From the analysis of each pattern, the local strain tensor is obtained following the above mentioned procedure. An example of the map of the tensor trace is given in Fig. 6. There are presently two ways of visually displaying the strain information, by associating to each investigated point the corresponding value of the component of the strain tensor (the trace in this case). In Fig. 6a the numerical value of the trace (in 1E-4 units) is shown, whereas the geometrical shape of the active region of the STI is superimposed to the two-dimensional map just to guide the eye. The data in Fig. 6b are deduced from exactly the same output file of ASAC as in Fig. 6a, but now the dots are given in colours, according to a selected palette (here blue and black indicate large and small compressive strains, respectively); to the map is superimposed the corresponding ADF-STEM micrograph. In the same way all the components of the strain tensor can be plotted as two-dimensional maps.

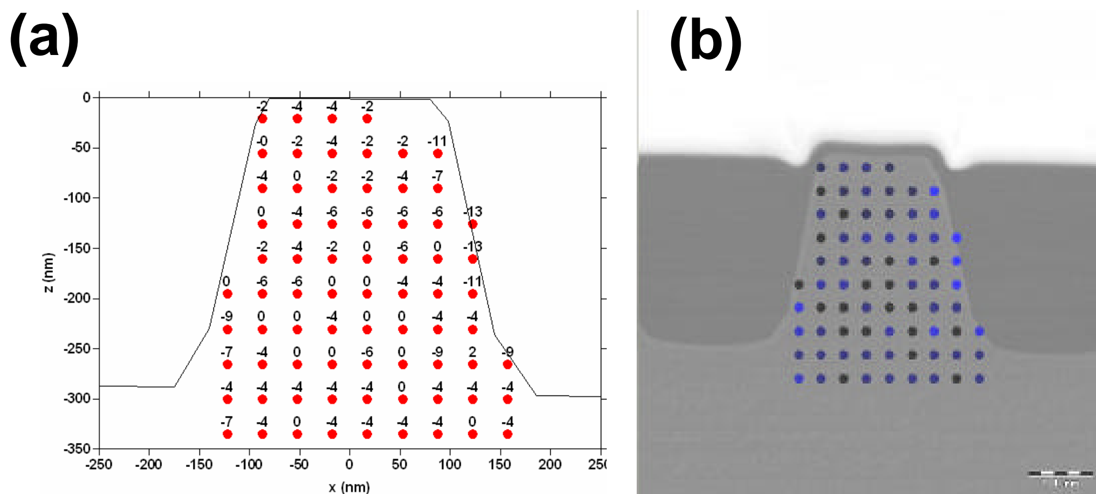

Figure 6. Maps of the tensor trace of the STI structure in Fig. 5. Measurements were performed in <340> orientation. In order to compare maps of active regions in differently processed STIs, each point can be associated with the corresponding numerical strain value (as in (a), 1E-4 units) or with different colours (as in (b), where blue and black correspond to large and small compressive strains, respectively). In (a) the profile of the shallow trenches is drawn to guide the eye. Note that by the ASAC software all the components of the strain tensor can be mapped. Adapted from (14).

Conclusions

The two STEM-based techniques described in this work (Z-contrast ADF and CBED) have proved to be very powerful in the quantitative analysis of dopant profiles in ultra-shallow junctions in silicon and of lattice strain mapping in STI structures, respectively. Their high spatial resolution and sensitivity make them very useful in the intercomparison of results obtained by different techniques, which is a key issue of the European project ANNA. In particular, it is planned to compare the dopant profiles with those obtained by SIMS (Secondary Ion Mass Spectrometry) and MEIS (Medium Energy Ion Scattering) advanced methodologies; likewise, the strain values obtained by CBED will be compared with the two dimensional process simulations currently employed in CMOS technology and the impact of strain on the electrical performances of the devices will be investigated.

Acknowledgments

This work is partially supported by the project ANNA (European Integrated **A**ctivity of Excellence and **N**etworking for **N**ano- and Micro-Electronics **A**nalysis) of the I3 initiative of the EU 6th Framework Programme.

References

1. P. Smeys, P.B. Griffin, Z.U. Rek, I. De Wolf and K.C. Saraswat, *IEEE Trans. Electron Dev.,* **46,** 1245 (1999)
2. S.J. Pennycook, S. D. Berger, and R. J. Culbertson, *J. Microsc.*,**144**, 229 (1986).
3. P.G. Merli, V. Morandi, and F. Corticelli, *Appl. Phys. Lett.*, **81**, 4535 (2002).
4. P.G. Merli, V. Morandi, G. Savini, M. Ferroni, and G. Sberveglieri, *Appl. Phys. Lett.*, **86**, 101916 (2005).
5. M. Ferri, S. Solmi, A. Parisini, M. Bersani, D. Giubertoni and M. Barozzi, *J. Appl. Phys.*, **99**, 113508 (2006).
6. A. Parisini, D. Giubertoni, M. Bersani, M. Ferri, V. Morandi, P. G. Merli, Proceedings of the 8th Multinational Congress on Microscopy, Prague, 18-21 june 2007, p. 43.
7. S.L. Elliott, R.F. Broom, and C.J. Humphreys, *J. Appl. Phys.*, 91, 9116 2002.
8. P.M.Jones, G.M.Rackham and J.W.Steeds, *Proc. R. Soc. Lond.*, **A 354**, 197 (1977).
9. Y.P. Lin, D.M. Bird and R. Vincent, *Ultramicroscopy*, **27**, 233 (1989).
10. ASAC: http://www.soft-imaging.com/en/164_190.htm
11. STREAM Contract No. IST-1999-10341 (http://stream.bo.cnr.it)
12. R.Balboni, S.Frabboni and A.Armigliato, *Phil. Mag.*, **A77**, 67 (1998)
13. Deliverable D2, STREAM project, p.25 (2000) (http://stream.bo.cnr.it